# A model of multicellular communication mediated through extracellular matrix microstructure

John Metzcar[1,2], Ben S. Duggan[3], Brandon Fischer[1], Matthew Murphy[2], Randy Heiland[1] and Paul Macklin[1*]

[1]Intelligent Systems Engineering, Indiana University, 700 N. Woodlawn, Bloomington, 47408, Indiana, United States of America.

[2]Informatics, Indiana University, 901 E. Tenth Street, Bloomington, 47408, Indiana, United States of America.

[3]Computer Science, Indiana University, 700 N. Woodlawn, Bloomington, 47408, Indiana, United States of America.

*Corresponding author(s). E-mail(s): macklinp@iu.edu;

Contributing authors: jpmetzca@iu.edu; bendugga@iu.edu; brandonfischer99@gmail.com; dmatthewmurphy@gmail.com; rheiland@iu.edu;

**Abstract**

Extracellular matrix (ECM) is a key part of the cellular microenvironment and critical in multiple disease and developmental processes. Representing ECM and cell-ECM interactions is a challenging multiscale problem. While several computational frameworks exist for ECM modeling, they typically focus on very detailed modeling of individual ECM fibers or represent only a single aspect of the ECM. Using the PhysiCell agent-based modeling platform, we developed a new framework of intermediate detail that addresses direct cell-ECM interactions. We represent a small region of ECM, an ECM element, with 3 variables: anisotropy, density, and orientation. We then place many ECM

elements throughout a space to form an ECM. Cells have a mechanical response to the ECM element variables and remodel ECM elements based on their velocity. We demonstrate aspects of this framework with a model of cell invasion where a cell's motility is driven by the ECM microstructure patterned by prior cells' movements. Investigating the limit of high-speed communication and with stepwise introduction of the framework features, we generate a range of cellular dynamics and ECM configurations – from recapitulating a homeostatic tissue, to indirect communication of paths (stigmergy), to collective migration. When we relax the high-speed communication assumption, we find that the behaviors persist but can be lost as rate of signal generation declines. This result suggests that cell-cell communication mediated via the ECM can constitute an important mechanism for collective cell behavior and multicellular pattern formation, with implications for tissue morphogenesis, developmental biology, microbial ecosystems, and cancer invasion.

**Keywords:** extracellular matrix, agent-based modeling, collective migration, stigmergy

# 1 Introduction

Cell-cell communication drives many processes, from cell migration and growth to diseases such as breast cancer [1, 2]. This communication occurs through many mechanisms (e.g. contact, paracrine, or endocrine signaling). It also occurs through indirect cellular signaling mechanisms such as the alteration of the tissue microenvironment. Changing the extracellular matrix (ECM), the materials that hold tissues together, is one of the commonly deployed indirect cell communication mechanisms [1, 3–8]. Through the ECM's physical properties, such as fiber orientations, it provides cues for cellular migration and can serve as a conduit to inhibit or promote cell migration [1, 4, 9–11]. For example, Carey et al. observed that fiber alignment induced anisotropic cell morphodynamics and spatial probing, guiding them along the axis of alignment while noting also that many questions remain unanswered regarding how cells navigate these environments [5]. In their review, Winkler et al. stated that remodeling of ECM can create paths leading cells out of ductal-carcinoma *in situ* [4]. Furthermore, signals from the ECM were implicated as influencing leader-follower migration, a form of collective cell movement where leader phenotype cells spearhead multicellular tissue invasion [12]. Multiple possible processes are shown to be at work in creating this leader-follower dynamic, with "action at a distance" via writing signals to the matrix as one possible mechanism ready for investigation [1, 12]. Overall, dysregulation of ECM maintenance is associated with disease processes, in particular aspects of cancer progression and metastasis [4, 11, 13]

Given the importance of ECM in biological processes, there are multiple frameworks for modeling and simulation of ECM and cell-matrix interactions [14]. Broadly, they can be placed in four categories: discrete force-based, continuous force-based, single field, or broad category of several paradigms which we refer to as "other".

Examples of the discrete force-based frameworks include where both the migrating cells and individual matrix fibers are embodied as agents with direct forces dictating motility and realignment respectively [15]. Macnamara et al. also adopt this paradigm and couple it with a model of blood vessel-cell interactions [16]. Other representations calculate forces over a network of individual spring-like elements. Zhu et al. construct ECM from a hook-and-spring network and Tozluoglu et al. model individual fiber filaments as hook-and-spring networks [17, 18]. Tsingos et al model a network of ECM fibers as a bead-spring chain model and couple this with a cellular-Potts individual cell model [19].

Continuous force-based models represent ECM as a continuously deformable material. Examples include van Oer et al., who use a finite element model of ECM coupled with a cellular-Potts model of cells and look at how stiffness and deformability of the ECM impact cell migration [20]. Ahmadzadeh et al. use a stress-strain relationship to deform fibers as well as incorporating cell adhesions to look at cellular level motility and morphology [21].

Single field (density) approaches to ECM often use partial-differential equations (PDEs) to update ECM density. Zeng et al. use a fibronectin "concentration" in developmental biology applications [22]. Daube et al. use a PDE for a scalar ECM density field in the context of sprouting angiogenesis in tumors [23]. Letort et al. use the PhyisBoSS framework, an implementation of PhyisCell [24] with the MaBoSS Boolean network simulator [25], to model cells while modeling ECM as a scalar-density field [26]. Trucu et al. model invasion as a moving value problem with ECM represented as a scalar field [27]. Building off of that work, Shuttleworth et al. 2019 and 2020 add non-local effects as well as orientation to the underlying moving boundary value of tumor invasion and adds matrix degradation respectively [28, 29].

Finally, there are other methods. Chauvier et al. and Hillen et al. use transport models to look at ECM [30, 31]. Other authors model ECM directly as a phase in an otherwise typical cellular-Potts model [32, 33]. Some authors also form long-range fibers by viewing sets of contiguous points occupied by ECM as fibers. This allows them to represent fiber orientation and length in addition to density [34, 35]. Finally Martinson et al. use a deposition of discrete ECM puncta followed by cellular realignment of the fibers to study collective migration of neural crest cells using both number of ECM puncta and their orientations to alter cell motion [36].

In this work, we take the approach of using a single phase of ECM with multiple variables (orientation, alignment, and density) modified via interactions

with cells, which we represent as individual agents. This approach gives a simulation more expression than a density field. However, it does not require the detailed knowledge, assumptions, or simulations of ECM components of other frameworks while still generating insights into multi-cellular interactions.

Furthermore, we developed a computational model of cellular invasion. It is a two phenotype leader-follower model, inspired by the cancer biology literature [12, 37]. Leaders communicate their paths to follower cells by altering the ECM microstructure. The followers read the ECM cues and various collective behaviors result depending on simulation parameters. Using this model, in the limit of high communication potential, we observe stigmergy and collective invasion. Relaxing this assumption, we still see these behaviors and note that they are sensitive to rates of microstructure remodeling (communication speed). This suggests that cell-cell communication mediated via the ECM can constitute an important mechanism and that other mechanisms, such as strong cell-cell adhesion or chemical signaling, may also be present to produce observed behaviors.

# 2 Methods

In this section, we first provide the conceptual background and formulation of the ECM and cell-ECM interactions framework (the ECM model). Then, we illustrate the framework with a series of computational experiments highlighting important aspects of the framework. Finally, we describe a model of cellular invasion used to explore our ECM model - a tumor spheroid simulation inspired by the cancer biology literature [12, 37]. For mathematical details, see Section 7.1 and 7.2.

## 2.1 ECM and cell-ECM interaction models

To enable explorations of ECM mediated cellular communication, we developed a three variable ECM representation and interaction rules for cells and the ECM. We use an agent-based approach to represent cells and a continuum model to represent the fine structure of ECM. Broadly, ECM elements are modified by cell movements and migration and in turn, cell motility is impacted by ECM element variables. Together, this constitutes a cell-cell communication method with the ECM microstructure modifications being the signal and changes in cell motility based on those changes the reading out of this signal.

### 2.1.1 Cell-based modeling framework

We use the PhysiCell tissue modeling system to implement the ECM and cell-ECM interactions models [24]. PhysiCell uses a center-based, off-lattice representation of cells and implements physical cell-cell mechanics. It takes a phenotypic approach to encoding cell behaviors letting each cell-agent carry

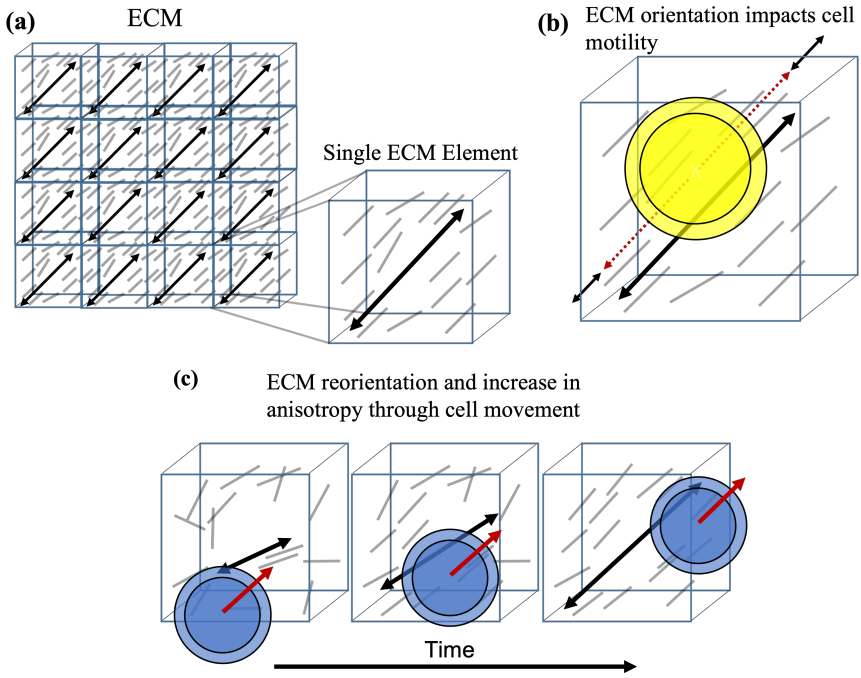


**Fig. 1**: **Schematic of ECM model and ECM based communication 1a** Illustrated here is an ECM, composed of tiled ECM elements. A single element contains many fibers (grey line segments) which we represent by an overall (average) fiber orientation and amount of self-alignment, or anisotropy (the black double-headed arrow and its length). **1b** An element's overall fiber orientation impacts a cell's motility, providing a preferred angle of travel through the element (dashed red arrow). The amount of influence is related to the amount of amount of anisotropy and the cell's ability to sense and respond to the ECM cues. **1c** Cell movement (cell direction - red arrow) remodels ECM by altering its elements' orientation and anisotropy. Cells align an element's orientation parallel to their direction of travel and increase anisotropy proportional to cell speed.

its own parameters and behavioral rules. To model the diffusive microenvironment, we use BioFVM, which comes with PhysiCell. BioFVM is a diffusion solver that uses a Cartesian representation of space and finite volume method to efficiently handle multiple diffusing substrates over tissue scale sized domains [38].

### 2.1.2 Extracellular matrix representation

Our model is intended to capture key aspects of a small region, or element, of ECM. We conceive of an element of ECM as having three variables: an average fiber orientation (*orientation*), a relative local fiber alignment correlation (*anisotropy*), and a quantity that captures the relative amount of material present in an element (*density*). Assembling many of these elements together makes a whole ECM. Figure 1a shows an ECM, which is comprised of tiled ECM elements. The inset shows a single element. It is conceived of as containing many fibers (grey line segments). However, the individual fibers are

unmodeled and instead fibers are represented as having an average orientation and anisotropy (the black double-headed arrow and its length) and volumetric density (illustrated as number of fibers per element in the schematic).

Mathematically, we center an element at a location $\mathbf{x}$ in space and define them as follows:

- ***Orientation:*** $\mathbf{f}(\mathbf{x})$, the average local fiber direction, represented as a unit length 3 dimensional vector.
- ***Anisotropy:*** $a(\mathbf{x})$, average local fiber alignment correlation (range 0 - 1). At zero, there is no correlation and at one, locally there is complete fiber-to-fiber correlation.
- ***Density:*** $\rho(\mathbf{x})$, volume fraction of fibers, which we will refer to as the average local fiber density (range 0 - 1). Zero refers to completely fluid filled and one to completely packed with fibers without void space.

Without a loss of generality, for our simulations and implementation, we arrange the elements in a Cartesian grid.

### 2.1.3 Cell-ECM interactions

We also model interactions between cells and the ECM. The conceptual model is below with the detailed mathematical model provided in Supplementary Material Sections 7.1 and 7.2.

*ECM impacts cell migration:*

- Fiber orientation provides directional cues.
- Anisotropy gives a strength of directional cue: high anisotropy increases an ECM element's influence on direction of cell migration.
- Density influences cell speed: too little ECM, cells have nothing to attach to; too much, cells cannot pass.

*Cell migration and movement impact microstructure:*

- Direction of cell migration reorients an ECM elements's orientation.
- Cell-ECM element contact increases ECM anisotropy proportional to cell speed.
- Cells remodel ECM density towards a target value.

The interactions between the ECM and cells can be specified at the cellular level, allowing for a variety of cell-ECM interaction phenotypes. Our framework captures the range of biological behaviors: cells may be very sensitive to ECM cues or unable to read them, may be equipped with the machinery to remodel ECM or not [12]. Finally, we note and will demonstrate that these features can be integrated with others such as sensitivity to chemical cues and cell-cell adhesion and to obtain an even richer range of cell behaviors.

## 2.2 Individual features of the cell-ECM communication model

Results in this section isolate and demonstrate a single or small number of aspects of the cell-ECM interaction model presented in Section 2.1. To aid in isolating only ECM-to-cell and cell-to-ECM effects, in this section we disabled cell-cell mechanical interactions by setting both the adhesion and repulsion parameters of the standard PhysiCell model to zero [24]. We used multiple cells per result to highlight the uniformity of interactions across the computational domain and as a visual aid rather than to explore how the cell-cell interactions may impact the simulations.

Note that while the framework does include an ECM density and its updates and influence on cell behavior, it is not highlighted in our examples. However, we include the description, methods, and assumptions for this aspect of the model for the sake of completeness of the framework and leave it to future work and others to highlight.

### 2.2.1 Cells produce signals in the ECM

***Combing the ECM: fiber orientation and alignment remodeling produces extended paths in the ECM***

Remodeling of the ECM units can produce paths that ECM sensitive cells can then follow. In Figure 2a, cells move deterministically across a field of un-oriented ECM aligning it in the direction of travel. Each ECM element is initialized with a random orientation and uniformly with $a = 0.9$. Remodeling cells move across the domain, producing individual changes in ECM elements as they travel. After 4 passes of writing signals to the matrix, the ECM is aligned almost completely parallel to the direction of travel with most elements' anisotropy having increased to approximately 0.92, producing preferred paths of transit across the domain. A video is linked in the Supplemental Materials (Section 7.4.1).

### 2.2.2 Cells read signals in the ECM, impacting their migration

All results in this section were produced with anisotropy and density uniformly set to 1.0 (maximum and most impactful value) and 0.5 (value of maximum cell speed) respectively and both the chemical and physical (ECM) environments not updating once initialized. This ensures that only dynamics between a cell and the ECM or respectively among a cell, ECM, and chemical field are isolated and other aspects held constant. Finally, the cells are highly sensitive to ECM ($s = 1.0$) as well as the chemical gradient ($b = 1.0$) when present.

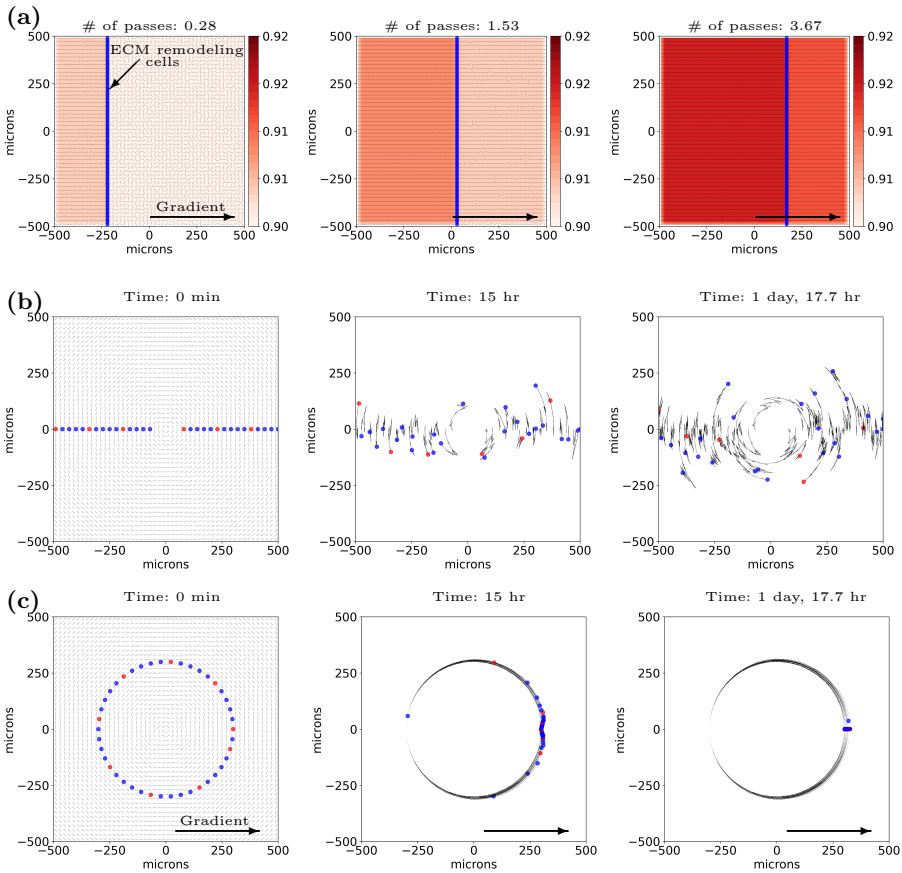


**Fig. 2**: **Highlights of individual aspects of the cell-ECM interactions:** (**2a - Remodeling**) A line of ECM remodeling cells (blue circles), motivated by a constant chemical gradient (black arrow), move in the positive x-direction, reorienting an initially random field of orientations (black line segments) with uniform anisotropy of 0.90 (left-most image in **2a**). Upon reaching the simulation boundary, the cells reset to the opposite boundary, and remodeling continues (middle - 2 passes). At 4 passes, the ECM is almost completely reoriented parallel to the direction of travel of the cells and anisotropy has increased from 0.90 to ∼0.92 (left). **2b, 2c - Reading ECM**. Both simulations use an ECM that is highly anisotropic ($a$ uniformly set to 1.0) and element orientations arranged to form approximate concentric circles. The simulation in **2b** begins with ECM senstive cells almost equally spaced along the line x=0 (left most image - cells shown in red and blue; color is for visual contrast only). Cells follow the ECM circles in an approximate 1-D random walk, forming circular arcs (small black arrows marking cell position history every 6 minutes). As the rate of curvature of ECM cues decreases away from the center of the computational domain, the cells better follow the ECM circles. The simulation in **2c** contrasts with **2b** by providing an additional environmental cue - a chemical gradient. As the ECM sensitive cells integrate both signals, in contrast to **2b**, their motion is no longer random and they travel uniformly in the direction of the gradient. With a circular initial configuration (left), the cells follow each other along the same circle (middle and right), coming to a point of meta-stability where the ECM orientation is exactly perpendicular to the chemical field. As in **2b**, cells "jump" off the path set by the ECM and overshooting their original path prior to a cell motility update.

### *Cells can closely follow paths in the ECM*

Supplementary Figure 2 shows influence of ECM on cell migration combined with a chemotactic field going to the right. The left-most subfigure shows the initial cell positions as well as the ECM element fiber orientations (45° and -45° from the x-axis in the top and bottom sections of the domain respectively). Without ECM influence, the cells would simply move to the right. Instead, the ECM biases the cell paths away from the path set by the gradient. The middle and right-most images include the cells positional history, shown as arrows trailing the blue and red cells (note in this and in all images in this section, the cell color is simply for visual contrast). A video is linked in the Supplemental Materials (Section 7.4.5).

### *Cells perform approximate 1-D random motion along ECM paths*

Figure 2b shows the results of cell motion on circular ECM. We show the initial cell configuration as well as the ECM element orientations on the left with the middle and right images including cell positional history at 15 hours and 41.7 hours simulated time respectively. We observed cells having no apparent preferred direction (approximately 1-D random motion) along the ECM circles, as expected given the lack of bias along ECM orientations. Because of the curved tracks, contrasting with Supplementary Figure 2, cells move off their initial circles out to ECM circles of higher radius. Note also that cells placed or traveling further from the origin more closely follow the underlying ECM cues. The circles furthest from the origin produce the best approximations to true circles, while further into the domain, the error between a true circle and the discretized ECM increases. Due to the high error at the center of the domain, for this simulation, we exclude the central region with radius of 80 $\mu$m or less. A video is linked in the Supplemental Materials (Section 7.4.1).

### *Cells can integrate environmental signals and follow non-linear paths*

Figure 2c shows the results of cell motion transitting circular ECM with an additional cue supplied by a chemical gradient. This additional information causes the cells to follow the ECM circle on which they were initially placed to the right (the direction of the chemical gradient). Note that at locations where the chemical gradient and ECM orientation are perpendicular, cells are in a quasi-stable state as the two directional cues cancel. This meta-stable state is seen in the lagging cell in the middle plot of Figure 2c. Note that all other cells in this plot, except the lagging blue cell on the left side of the image, have moved many cell lengths from their initial positions. This cell began at the x-axis, which defines a line in which all units of ECM have an orientation perpendicular to the chemical field. Likewise, all the cells converge at the x-axis, where their initial ECM contour becomes perpendicular to the chemical field. Finally, as in Figure 2b, we observe mild "track jumping" as the cells

do not converge to a single point, despite having all begun equidistant from the origin (on a shared circle of ECM). A video is linked in the Supplemental Materials (Section 7.4.1).

## 2.3 Cell invasion model

To explore our cell-ECM communication model in a rich setting and address questions centered on the mechanisms of tumor cell invasion, we developed a tissue simulation focusing on invasive cellular behavior. It is inspired by the cancer biology literature [12, 37] and builds off of previous cell-based spheroid modeling work [24]. Mimicking Cheung et al[12], we include two cell phenotypes - leader cells endowed with more invasive behaviors (directed outward motility and ignorance to ECM cues) and follower cells with less invasive behaviors (random motility, responsive to ECM and chemotactic cues). Their observations suggest some form of communication between the leaders and followers; we model that communication as signals written in and read from ECM microstructure. We use our cell-ECM interaction model with leaders producing signals (remodeling) and followers reading them. Simulating these phenotypes and interactions lets us explore and test for the microenvironmental conditions and behaviors required for collective migration. The simulation was implemented in PhysiCell 1.4.1 as a 2-D simulation (single slice of a 3-D environment). Brief details on each component of these simulations follow.

**Table 1**: **Cell-based model:** principle behaviors, parameters, and systems effects

| Phenotype | Behavior | Key parameter(s) | Key outputs |
|---|---|---|---|
| Leader cells | ECM remodeling | Cellular rate of matrix realignment, rate of anisotropy growth | Lays cues for followers to sense |
| | Chemotaxis | Bias | Enables production of coherent paths |
| | Cell-cell adhesion and repulsion | Ratio of adhesion strength to repulsion strength | Enables collective cell migration |
| Follower cells | ECM sensing | Cell ECM sensitivity | Allows cells to use cues in the ECM |
| | Chemotaxis | Bias | Enables coherent migration |
| | Cell-cell adhesion and repulsion | Ratio of adhesion strength to repulsion strength | Enables collective cell migration |
| | Random motion | - | Enables finding of paths in the ECM |

### 2.3.1 Cellular modeling

We model two different phenotypes - leader cells and follower cells. These cells represent invasive and non-invasive cancer cells, respectively. The key rules of the leader-follower model are summarized in Table 1. In particular, leader cells follow oxygen gradients with a high chemotactic bias ($b_l = 0.95$) (Model I - Equation 15) and encode their movements via ECM remodeling (see Section 7.1 for details). Followers movements are heavily influenced by signals in the ECM and chemotactic when in anisotropic ECM (Model II - Equation 16 - see Section (7.2 for mathematical details). They read signals in the ECM with a high sensitivity ($s = 1.0$) and are incapable of remodeling ECM. Thus, in highly anisotropic ECM, followers follow ECM dictated paths up the chemical gradient while in unaligned ECM, they move randomly. For implementation, we used the default cell phenotype from PhysiCell. To ensure that the physical interactions among the cells and their environment are driving dynamics, we do not allow cell proliferation or death. In general, unless otherwise noted, the cells were initialized with the default values and functions from PhysiCell. See the Supplemental Material Table 2 for additional parameter values.

### 2.3.2 Tissue microenvironment

We employ the native reaction-diffusion-decay simulator in Physicell, BioFVM, [38] to simulate the chemical microenvironment. We simulate avascular tissue with a diffusing oxygen-like field coming from the domain boundaries (Dirichlet conditions). Cells uptake oxygen and there is decay in the cellular milieu. Unless otherwise specified, we use default values from PhysiCell/BioFVM. Those values give a diffusion length scale of 100 $\mu$m for regions of high cell density. We pre-condition the domain by running the diffusion solver for 10 simulated minutes before starting cellular simulation. See Supplemental Material Table 3 for additional details.

For ECM, we use the model described in Section 2.1. We place the ECM elements overlaying the BioFVM voxels exactly unless otherwise noted. The two meshes explicitly have a shared origin and coordinate system. The ECM is initialized uniformly as completely isotropic, of ideal density for cellular motion ($\rho = 0.5$), and with random fiber orientations. See Supplemental Material Table 4 for additional details.

### 2.3.3 Tissue

Cells are placed at the center of the computational domain in a circular region of radius 175 $\mu$m and randomly assigned to be either followers or leaders. Cells are initialized at equilibrium spacing with six neighbors (hexagonal packing). See the Supplemental Material Table 5 for additional details.

### 2.4 Computational method details and data availability

This work implemented and run in PhysiCell 1.4.1 [24]. All codes are available with a permissive BSD license, including the ECM extensions, at GitHub with release located here. A free, interactive cloud-hosted version of the cell invasion model, using the ECM and cell-ECM frameworks, is available at nanoHUB.

We performed model exploration using DAPT 0.9.2. DAPT is a straightforward way to organize model exploration on a mixed compute resources for small teams. For more information see Duggan et al [39].

We used xml2jupyter to transform this command line C++ code into a Jupyter notebook-based graphical user interface [40]. This version is the interface deployed at nanoHUB.

Simulation data is available upon reasonable request.

## 3 Cell invasion simulations and multicellular communication

### 3.1 Signal generation and reading are required for collective behavior

Isolating two model rules, the ability to produce and read signals, while also allowing cell-cell repulsion, we saw that both ECM microstructure (signal generation) and ECM sensitivity (environmental reading) are required for collective migration. In Figure 3, we observe similar behavior of leaders and followers with ECM writing only (left column) and ECM reading only (middle column) simulations. Leaders separate from the initial disc of cells and reach the simulation boundary around 16 hours while followers remain roughly in the center of the domain. Only with both writing and reading (right column), were most cells able to escape the domain center and invade their surroundings. Here, we observed stigmergy, a form of collective behavior produced by indirect communication where signals encoded by agents enable other agents to follow the first agents' paths. Links to simulation videos are in Section 7.4.2.

### 3.2 Cell-cell adhesion is required to enable collective migration

Adding cell-cell adhesion, we observed a range of tissue morphologies, including collective migration. With cell-cell adhesion present and varying cell speed, we see that ECM mediated communication can still produce stigmergy (Figure 4a). In Figure 4b, we see that leaders have migrated to the leading edge of clumps of mostly follower cells. Cells generally stay in contact with each other, producing leader-follower collective invasion. Finally, when cell speed is even

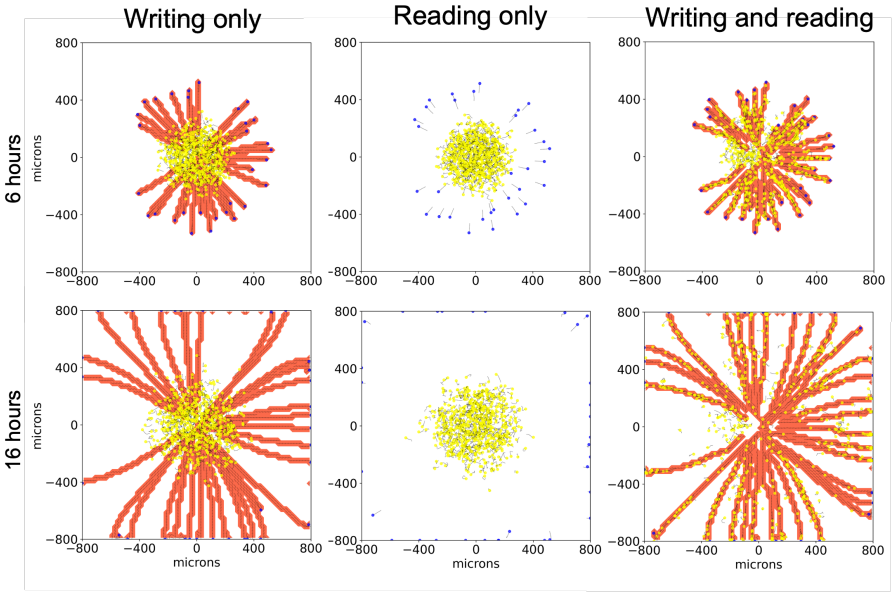


**Fig. 3**: **Communication of cell path through environmental modification produces invasive, stigmergic cell behavior:** Modification of the environment (left) and reading of the environmental signals (middle) separately do not produce collective behavior. With both together (right column) we observe that most cells escape the domain center and invade their surroundings via stigmergy. Initial configuration - 703 agents (5 % leaders) in 175 $\mu$m circle. Yellow agents: followers. Blue agents: leaders. Red contour plot: ECM anisotropy - uniformly equal to one in remodeled ECM elements. Line segments: ECM orientation. Black arrows: cell positional history, going back 12 time points (sampled every 6 minutes).

lower, adhesion takes over cell mechanics and tissue morphology is constant over the computational experiment (Figure 4c). Links to simulation videos are in Section 7.4.3.

## 3.3 Collective migration is retained in the context of delayed communication

Having shown that the cell-ECM model is capable of producing a range of behaviors in the limit of high communication speed, we relax this limit assumption. Figure 5 contrasts the results of the limit of instant signal writing with finite signal writing. Figure 5a shows two time points using the limit model, with cell speed of 0.5 $\mu$m/min and adhesion value of 10 $\mu$m/min. In the earlier time point (top), we see what was the initial cluster of cells broken into several smaller clusters moving out from the center of the domain. In the next time point, we see that heterogenous clusters have continued towards the simulation boundary (with some reaching it) while a cluster of followers remains in the middle. This is a direct leader-follower migration with several coherent mixed clusters invading the area around the initial disc of cells. In Figure 5b, relaxing instantaneous signal writing, we observe that collective migration

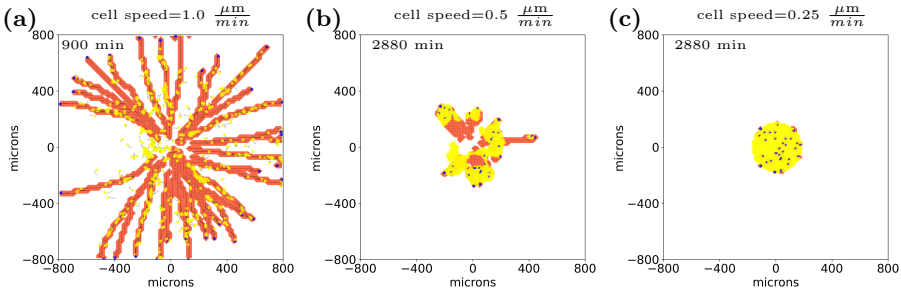


**Fig. 4**: **Multiple behaviors are produced with cell-ECM model:** With cell-cell adhesion on (adhesion = 10 $\frac{\mu m}{min}$), multiple behavioral regimes are observed in the limit case of high writing potential. In **(a)** we see stigmergy with followers (yellow cells) following trails left by leaders (blue cells), as in Figure 3. Decreasing the cell speed by half to 0.5 $\frac{\mu m}{min}$ yields collective migration **(b)**. In **(c)** with cell speed again halved (s=0.25 $\frac{\mu m}{min}$), cell-cell adhesion cannot be overcome and the tissue morphology is frozen in the initial configuration. Initial configuration - 703 agents (5 % leaders) in 175 $\mu$m circle. Adhesion set to 10 $\frac{\mu m}{min}$. Yellow agents: followers. Blue agents: leaders. Red contour plot: ECM anisotropy - uniformly equal to one in remodeled ECM elements. Line segments: ECM orientation. Black arrows: cell positional history, going back 12 time points (sampled every 6 minutes).

still occurs. Leaders remain in contact with followers and lead them out of the center of the domain. As the signals to followers are not as uniform or strong leading to less coherent migration, the leaders break away and do not stay in contact as long as in the contrasting simulation. Because of delays created by finite time ECM remodeling, the ECM based communication signals are relatively lacking in strength. Interestingly, overall migration appears to actually be enhanced with leaders pulling out cells behind them before finally breaking away. Then the remaining followers continue out behind the leaders via stigmergic behavior. See for Supplementary Section 7.4.4 for links to videos.

Collective migration behavior in the finite signal writing scenario is sensitive to remodeling parameters and is lost with a less than order of magnitude change in them as seen in Supplementary Figure 3. Fiber reorientation and realignment rates vary by a factor of 4 are enough to change the behavior.

# 4 Discussion

In this work, we presented a new mathematical and computational framework of multicellular communication mediated through ECM microstructure. As cells move, they modify the ECM and change behaviors in response to cues generated by those modifications, enabling communication of their paths. The framework captures multiple aspects of ECM (orientation, correlation of fiber-fiber self-alignment, and density) in a single field - an array of ECM elements. After showing model behavior for individual agents, we investigated a cellular invasion model inspired by the observations of leader-follower behavior in breast cancer [12]. We explored the leader-follower model by looking at the

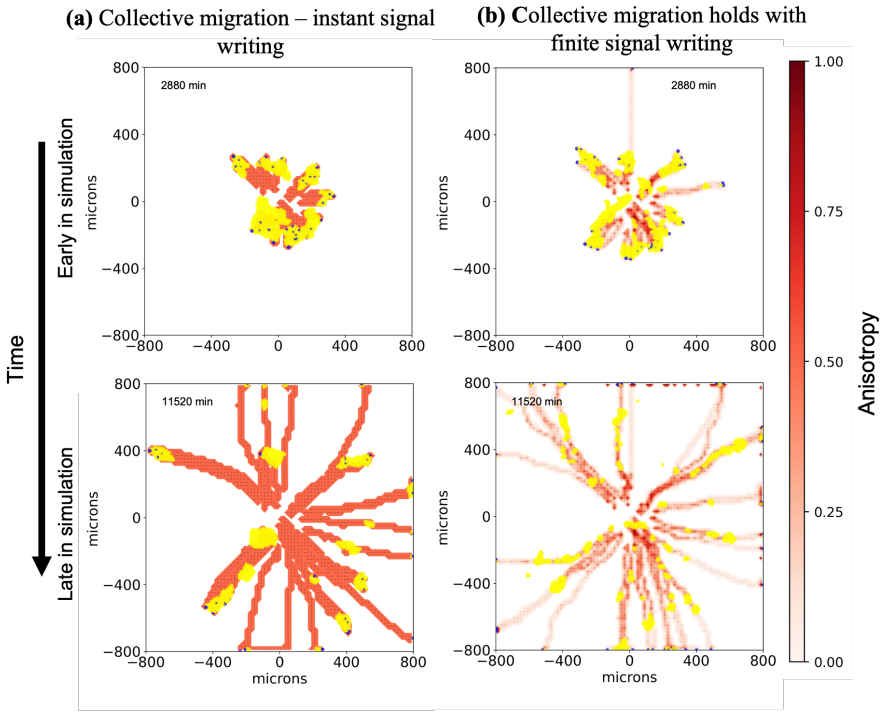


**Fig. 5**: **Collective migration is retained in the context of delayed communication** In the limit of instant signal generation, we see collective migration with mixed clumps of both leader (blue) and follower (yellow) cells migrating together (**(5a)** and Fig 4**b**). As seen in (**5b**), this behavior is robust to non-instant signal writing (modification of ECM variables). Leaders stay in contact with followers and lead them out of the center of the domain. They do not stay in contact as long as in **(5a)** but strong enough paths are generated to enable followers to continue out via stigmergy. This behavior is sensitive to remodeling parameters and is lost with a less than order of magnitude change in them. See Supplementary Material Figure 3. Fiber realignment rate: 0.004 $\text{min}^{-1}$, fiber reorientation rate: 4 $\text{min}^{-1}$. Initial configuration - 703 agents (5 % leaders) in 175 $\mu$m circle. Adhesion set to 10 $\frac{\mu m}{min}$. Yellow agents: followers. Blue agents: leaders. Contour plots: ECM anisotropy - (**(5a)**) uniformly equal to one in remodeled ECM elements and (**(5b)** color bar. Line segments: ECM orientation. Black arrows: cell positional history, going back 12 time points (sampled every 6 minutes).

limit of high fidelity communication, using an instantaneous rate of writing signals through ECM modification. Through iterative layering of interactions, we showed that the invasive cell model required ECM mediated communication to produce collective behavior (stigmergy) and furthermore required cell-cell adhesion to enable collective invasion. We observed that the collective behavior was sensitive to delays and signal strength with collective invasion possible for a range of remodeling rates but not guaranteed.

Figure 2 and accompanying videos (see Supplemental Material Section 7.4.1) demonstrate features of our cell-ECM interaction model and show the correspondence between expected and actual behaviors of the model. The ECM is remodelable by cell agents (Figure 2a) and can influence cell migration. Supplementary Figure 2 and Figure 2b and c highlight important aspects of how

agent motility and environmental cues interact. Figure 2b shows that cells may miss ECM cues, especially in regions of high curvature. If cell agents completely traverse an ECM element prior to a motility update and the next cue they read is greatly out of line with the previous cue, the cells will miss the path. This shows that in our model, paths of high curvature (with respect to the cell persistence time and speed) may be missed. Figure 2c demonstrates another interesting aspect of our cell-ECM framework. If a cell receives two equally influencing and mutually perpendicular cues, it can become stuck. This is an extreme condition as in a typical simulation, we would not expect that an agent could achieve a perfect alignment of an ECM element and a conflicting cue. Without a perfect alignment, the agent will slow at that location, but will not stop. Overall, these model demonstrations show that on highly anisotropic ECM, ECM sensitive cells can perform approximate 1-D random motion (Figure 2b) while when given an additional cue, unidirectional motility appears (Figure 2d and Supplementary Figure 2).

With the strong signals laid by instant remodeling of the ECM, we observed two kinds of collective behavior realized via ECM-based communication - stigmergy and collective migration in Figures 3 and 4. These behaviors, in particular collective migration, were also observed when the communication rate was reduced to finite time scales (Figure 5b). Unexpectedly, overall escape from the center of the domain appears to be enhanced with slower signal writing, likely due to the cells' enhanced ability to move independently which facilitates both leader-follower and stigmergic migration. However, decreasing rates within one order of magnitude from the rates in Figure 5b, forms of collective behavior were no longer observed (Supplementary Figure 3). This suggests that in the cases where signal generation is slow compared to cell speeds, ECM mediated communication is important and that other mechanisms compensate when collective behaviors are observed.

We observed that we needed to give the follower cells an additional bias beyond cell-cell contact to allow them to move as one along the cues written in the ECM. In our model, we use oxygen chemotaxis in the follower cell population. In reality, it could also be a chemotactic cue coming from the leaders, some matrix factor the leaders release, or some other cue [4, 12].

Also, our current cell modeling framework does not allow for asymmetric rates of cell-cell attachment nor asymmetric adhesion such that a follower might have a different adhesion strength to a follower versus a leader phenotype cell. Introducing spring-like attachments with different rates of attachment versus detachment would better mimic actual cell adhesion [41]. This enhanced adhesion might facilitate the ability of ECM signals to enable collective migration, even in the absence of an additional directional cue such as an oxygen gradient.

We note that our model of ECM captures only local remodeling. This contrasts with other models' ability to capture the network like connections within a full ECM (eg - [17]). To produce a computationally efficient ECM, we accept this

limit. In the future, we may explore spreading remodeling over multiple ECM elements, for example with Gaussian smoothing.

## 5 Funding

We thank the Jayne Koskinas Ted Giovanis Foundation for Health and Policy and Breast Cancer Research Foundation for generous support. Additionally, this work was partially supported by the National Science Foundation (Grants 1735095 and 1720625).

## 6 Acknowledgements

We would like to thank Michael Getz, Adrianne Jenner, and Jordan Rozum for their expertise and assistance with this work. We gratefully acknowledge access to FutureSystems at the Digital Science Center, Luddy School of Informatics, Computing, and Engineering.

## References

[1] Cheung, K.J., Ewald, A.J.: Illuminating breast cancer invasion: Diverse roles for cell–cell interactions. Current Opinion in Cell Biology **30**, 99–111 (2014). https://doi.org/10.1016/j.ceb.2014.07.003

[2] Hanahan, D., Weinberg, R.A.: Hallmarks of Cancer: The Next Generation. Cell **144**(5), 646–674 (2011). https://doi.org/10.1016/j.cell.2011.02.013

[3] Humphrey, J.D., Dufresne, E.R., Schwartz, M.A.: Mechanotransduction and extracellular matrix homeostasis. Nature Reviews Molecular Cell Biology **15**(12), 802–812 (2014). https://doi.org/10.1038/nrm3896

[4] Winkler, J., Abisoye-Ogunniyan, A., Metcalf, K.J., Werb, Z.: Concepts of extracellular matrix remodelling in tumour progression and metastasis. Nature Communications **11**(1), 5120 (2020). https://doi.org/10.1038/s41467-020-18794-x

[5] Carey, S.P., Goldblatt, Z.E., Martin, K.E., Romero, B., Williams, R.M., Reinhart-King, C.A.: Local extracellular matrix alignment directs cellular protrusion dynamics and migration through Rac1 and FAK. Integrative Biology **8**(8), 821–835 (2016). https://doi.org/10.1039/C6IB00030D

[6] Frantz, C., Stewart, K.M., Weaver, V.M.: The extracellular matrix at a glance. Journal of Cell Science **123**(24), 4195–4200 (2010). https://doi.org/10.1242/jcs.023820

[7] LeBleu, V.S., MacDonald, B., Kalluri, R.: Structure and Function of Basement Membranes. Experimental Biology and Medicine **232**(9), 1121–1129 (2007). https://doi.org/10.3181/0703-MR-72

[8] Macklin, P., Edgerton, M.E., Thompson, A.M., Cristini, V.: Patient-calibrated agent-based modelling of ductal carcinoma in situ (DCIS): From microscopic measurements to macroscopic predictions of clinical progression. Journal of Theoretical Biology **301**, 122–140 (2012). https://doi.org/10.1016/j.jtbi.2012.02.002

[9] Werb, Z., Sympson, C.J., Alexander, C.M., Thomasset, N., Lund, L.R., MacAuley, A., Ashkenas, J., Bissell, M.J.: Extracellular matrix remodeling and the regulation of epithelial-stromal interactions during differentiation and involution. Kidney international. Supplement **54**, 68–74 (1996)

[10] Ewald, A.J., Brenot, A., Duong, M., Chan, B.S., Werb, Z.: Collective Epithelial Migration and Cell Rearrangements Drive Mammary Branching Morphogenesis. Developmental Cell **14**(4), 570–581 (2008). https://doi.org/10.1016/j.devcel.2008.03.003

[11] Lu, P., Takai, K., Weaver, V.M., Werb, Z.: Extracellular Matrix Degradation and Remodeling in Development and Disease. Cold Spring Harbor Perspectives in Biology **3**(12), 005058–005058 (2011). https://doi.org/10.1101/cshperspect.a005058

[12] Cheung, K.J., Gabrielson, E., Werb, Z., Ewald, A.J.: Collective Invasion in Breast Cancer Requires a Conserved Basal Epithelial Program. Cell **155**(7), 1639–1651 (2013). https://doi.org/10.1016/j.cell.2013.11.029

[13] Nguyen-Ngoc, K.-V., Cheung, K.J., Brenot, A., Shamir, E.R., Gray, R.S., Hines, W.C., Yaswen, P., Werb, Z., Ewald, A.J.: ECM microenvironment regulates collective migration and local dissemination in normal and malignant mammary epithelium. Proceedings of the National Academy of Sciences **109**(39), 2595–2604 (2012). https://doi.org/10.1073/pnas.1212834109

[14] Metzcar, J., Wang, Y., Heiland, R., Macklin, P.: A Review of Cell-Based Computational Modeling in Cancer Biology. JCO Clinical Cancer Informatics (3), 1–13 (2019). https://doi.org/10.1200/CCI.18.00069

[15] Schlüter, D.K., Ramis-Conde, I., Chaplain, M.A.J.: Computational Modeling of Single-Cell Migration: The Leading Role of Extracellular Matrix Fibers. Biophysical Journal **103**(6), 1141–1151 (2012). https://doi.org/10.1016/j.bpj.2012.07.048

[16] Macnamara, C.K., Caiazzo, A., Ramis-Conde, I., Chaplain, M.A.J.: Computational modelling and simulation of cancer growth and migration within a 3D heterogeneous tissue: The effects of fibre and vascular structure. Journal of Computational Science **40**, 101067 (2020). https://doi.org/10.1016/j.jocs.2019.101067

[17] Zhu, J., Mogilner, A.: Comparison of cell migration mechanical strategies in three-dimensional matrices: A computational study. Interface focus **6**(5), 20160040 (2016). https://doi.org/10.1098/rsfs.2016.0040

[18] Tozluoğlu, M., Tournier, A.L., Jenkins, R.P., Hooper, S., Bates, P.A., Sahai, E.: Matrix geometry determines optimal cancer cell migration strategy and modulates response to interventions. Nature Cell Biology **15**(7), 751–762 (2013). https://doi.org/10.1038/ncb2775

[19] Tsingos, E., Bakker, B.H., Keijzer, K.A.E., Hupkes, H.J., Merks, R.M.H.: Modelling the Mechanical Cross-Talk between Cells and Fibrous Extracellular Matrix Using Hybrid Cellular Potts and Molecular Dynamics Methods. bioRxiv (2022). https://doi.org/10.1101/2022.06.10.495667

[20] van Oers, R.F.M., Rens, E.G., LaValley, D.J., Reinhart-King, C.A., Merks, R.M.H.: Mechanical Cell-Matrix Feedback Explains Pairwise and Collective Endothelial Cell Behavior In Vitro. PLOS Computational Biology **10**(8), 1003774 (2014). https://doi.org/10.1371/journal.pcbi.1003774

[21] Ahmadzadeh, H., Webster, M.R., Behera, R., Jimenez Valencia, A.M., Wirtz, D., Weeraratna, A.T., Shenoy, V.B.: Modeling the two-way feedback between contractility and matrix realignment reveals a nonlinear mode of cancer cell invasion. Proceedings of the National Academy of Sciences **114**(9), 1617–1626 (2017). https://doi.org/10.1073/pnas.1617037114

[22] Zeng, W., Thomas, G.L., Glazier, J.A.: Non-Turing stripes and spots: A novel mechanism for biological cell clustering. Physica A: Statistical Mechanics and its Applications **341**, 482–494 (2004). https://doi.org/10.1016/j.physa.2004.03.089

[23] Daub, J.T., Merks, R.M.H.: A Cell-Based Model of Extracellular-Matrix-Guided Endothelial Cell Migration During Angiogenesis. Bulletin of Mathematical Biology **75**(8), 1377–1399 (2013). https://doi.org/10.1007/s11538-013-9826-5

[24] Ghaffarizadeh, A., Heiland, R., Friedman, S.H., Mumenthaler, S.M., Macklin, P.: PhysiCell: An open source physics-based cell simulator for 3-D multicellular systems. PLOS Computational Biology **14**(2), 1005991 (2018). https://doi.org/10.1371/journal.pcbi.1005991

[25] Stoll, G., Caron, B., Viara, E., Dugourd, A., Zinovyev, A., Naldi, A., Kroemer, G., Barillot, E., Calzone, L.: MaBoSS 2.0: An environment for stochastic Boolean modeling. Bioinformatics **33**(14), 2226–2228 (2017). https://doi.org/10.1093/bioinformatics/btx123

[26] Letort, G., Montagud, A., Stoll, G., Heiland, R., Barillot, E., Macklin, P., Zinovyev, A., Calzone, L.: PhysiBoSS: A multi-scale agent-based modelling framework integrating physical dimension and cell signalling. Bioinformatics **35**(7), 1188–1196 (2019). https://doi.org/10.1093/bioinformatics/bty766

[27] Trucu, D., Lin, P., Chaplain, M.A.J., Wang, Y.: A Multiscale Moving Boundary Model Arising in Cancer Invasion. Multiscale Modeling & Simulation **11**(1), 309–335 (2013). https://doi.org/10.1137/110839011

[28] Shuttleworth, R., Trucu, D.: Multiscale Modelling of Fibres Dynamics and Cell Adhesion within Moving Boundary Cancer Invasion. Bulletin of Mathematical Biology **81**(7), 2176–2219 (2019). https://doi.org/10.1007/s11538-019-00598-w

[29] Shuttleworth, R., Trucu, D.: Cell-Scale Degradation of Peritumoural Extracellular Matrix Fibre Network and Its Role Within Tissue-Scale Cancer Invasion. Bulletin of Mathematical Biology **82**(6), 65 (2020). https://doi.org/10.1007/s11538-020-00732-z

[30] Chauviere, A., Hillen, T., Preziosi, L.: Modeling cell movement in anisotropic and heterogeneous network tissues. Networks & Heterogeneous Media **2**(2), 333–357 (2007). https://doi.org/10.3934/nhm.2007.2.333

[31] Hillen, T.: M5 mesoscopic and macroscopic models for mesenchymal motion. Journal of Mathematical Biology **53**(4), 585–616 (2006). https://doi.org/10.1007/s00285-006-0017-y

[32] Rubenstein, B.M., Kaufman, L.J.: The Role of Extracellular Matrix in Glioma Invasion: A Cellular Potts Model Approach. Biophysical Journal **95**, 5661–5680 (2008). https://doi.org/10.1529/biophysj.108.140624

[33] Scianna, M., Preziosi, L., Wolf, K.: A Cellular Potts model simulating cell migration on and in matrix environments. Mathematical Biosciences and Engineering **10**(1), 235–261 (2013). https://doi.org/10.3934/mbe.2013.10.235

[34] Szabó, A., Varga, K., Garay, T., Hegedűs, B., Czirók, A.: Invasion from a cell aggregate—the roles of active cell motion and mechanical equilibrium. Physical Biology **9**(1), 016010 (2012). https://doi.org/10.1088/1478-3975/9/1/016010

[35] Kumar, S., Kapoor, A., Desai, S., Inamdar, M.M., Sen, S.: Proteolytic and non-proteolytic regulation of collective cell invasion: Tuning by ECM density and organization. Scientific Reports **6**(1), 19905 (2016). https://doi.org/10.1038/srep19905

[36] Martinson, W.D., McLennan, R., Teddy, J.M., McKinney, M.C., Davidson, L.A., Baker, R.E., Byrne, H.M., Kulesa, P.M., Maini, P.K.: Dynamic Fibronectin Assembly and Remodeling by Leader Neural Crest Cells Prevents Jamming in Collective Cell Migration. arXiv (2022). https://doi.org/10.48550/arXiv.2209.07794

[37] Carey, S.P., Starchenko, A., McGregor, A.L., Reinhart-King, C.A.: Leading malignant cells initiate collective epithelial cell invasion in a three-dimensional heterotypic tumor spheroid model. Clinical & Experimental Metastasis **30**(5), 615–630 (2013). https://doi.org/10.1007/s10585-013-9565-x

[38] Ghaffarizadeh, A., Friedman, S.H., Macklin, P.: BioFVM: An efficient, parallelized diffusive transport solver for 3-D biological simulations. Bioinformatics **32**(8), 1256–1258 (2016). https://doi.org/10.1093/bioinformatics/btv730

[39] Duggan, B., Metzcar, J., Macklin, P.: DAPT: A package enabling distributed automated parameter testing. Gigabyte **2021**, 1–10 (2021). https://doi.org/10.46471/gigabyte.22

[40] Heiland, R., Mishler, D., Zhang, T., Bower, E., Macklin, P.: Xml2jupyter: Mapping parameters between XML and Jupyter widgets. Journal of Open Source Software **4**(39), 1408 (2019). https://doi.org/10.21105/joss.01408

[41] Ozik, J., Collier, N., Heiland, R., An, G., Macklin, P.: Learning-accelerated Discovery of Immune-Tumour Interactions. Preprint, Systems Biology (March 2019). https://doi.org/10.1101/573972

# 7 Supplementary Material

## 7.1 Cell remodeling of ECM microstructure: Signal writing

Here we detail the mathematical models for updating ECM anisotropy, orientation, and density - the methods of writing a signal to the matrix. The ECM elements and cells are conceived of as being in close contact; cells alter the ECM element they are physically in. To formalize which ECM element a cell modifies out of the many possible options (see Figure 1a), we define cells as interacting with whichever element their center coordinates are the closest to, as in [24]. To do this, suppose cell $i$ is at position $\mathbf{x_i}$. We remodel the ECM element whose center is closest to $\mathbf{x_i}$. We outline two related methods for writing signals - the limit case of instantaneous signal writing and the non-instantaneous case.

### *Limit of high writing potential*

To explore an extreme case of ECM mediated communication, we model anisotropy and ECM element orientation as being immediately remodeled when contacted by a remodeling cell, resulting in the following relationships to update $a$ and $\mathbf{f}$:

$$a(\mathbf{x_i}) = 1 \tag{1}$$

$$\mathbf{f}(\mathbf{x_i}) = \mathbf{d_{remodeler}}. \tag{2}$$

Because of the underlying updates to $\mathbf{f}$ (see next subsection), this permanently writes with high signal strength the direction of travel of the first cell to pass through a particular ECM element.

### *Non-instantaneous signal writing*

#### *Anisotropy*

Anisotropy is represented by a scalar ranging from 0 to 1, representing "complete lack of anisotropy" (or a disordered state) to "complete anisotropy" (a highly ordered state). The rate of change in anisotropy over time is given as:

$$\frac{da(\mathbf{x_i})}{dt} = r_a(1 - a(\mathbf{x_i})). \tag{3}$$

$r_a$ is specified as:

$$r_a = r_{a0} s_{\text{cell}} \tag{4}$$

where $\mathrm{r}_{a0}$ is a base rate of change and $s_{\text{cell}}$ is the migration speed of the cell changing the ECM anisotropy.

### *Orientation*

We model changes to fiber orientation as follows:

$$\frac{d\mathbf{f}(\mathbf{x_i})}{dt} = -r_f \left( \mathbf{f}(\mathbf{x_i}) - \frac{\mathbf{d_{remodeler}}}{||\mathbf{d_{remodeler}}||} \right) \tag{5}$$

with

$$r_f = r_{f0} s_{\text{cell}}(1-a). \tag{6}$$

$\mathrm{r}_{f0}$ is the base rate of change, $\mathbf{d_{remodeler}}$ is the direction of the remodeling cell, and $s_{\text{cell}}$ is cell speed. $\boldsymbol{f}$ is normalized after each update. Note that when $a = 1$, orientation cannot change.

### *Density*

Density ranges from 0 to 1, representing fluid filled tissue to very dense tissue completely filled with fibers, respectively. Cells change ECM density locally through the following relationship:

$$\frac{d\rho(\mathbf{x_i})}{dt} = r_{density}(\rho_{target} - \rho(\mathbf{x_i})) \tag{7}$$

where $r_{density}$ is the cell's characteristic rate of deposition/degradation of ECM and $\rho_{target}$ is the cell's target for ECM density.

## 7.2 ECM microstructure influence on cell motility: Signal reading

Cell motion, in particular, cell speed and direction, can be altered via cell-ECM interactions. In a multicellular environment, this is the receiving step of communication enabling cells to communicate their paths to other cells. ECM element orientation and anisotropy are combined with a cell's preferred direction to produce the cell motility vector. Independently, cell speed is influenced by ECM density. We layout the orientation and anisotropy influences first, then the influence of density. As with writing signals to the ECM, we define cells to be in and read whichever element their center coordinates are the closest to, as in [24].

### *ECM orientation and anisotropy*

We developed a method to calculate $\mathbf{d_{actual}}$, a cell's actual motility direction, based on the cell's preferred direction $\mathbf{d_{preferred}}$, a cell specific ECM sensitivity $s$, and local anisotropy and orientation. As illustrated in Supplementary Figure 1, we want to constrain cell motion to the sector spanning the ECM orientation ($\mathbf{f}$) and the cell's intended direction of travel ($\mathbf{d_{preferred}}$) in a way that does not bias direction of travel along the fibers. We use $\mathbf{f}$ and $\mathbf{d_{preferred}}$ to form an orthonormal basis set that spans the cell's potential directions (the sector produced by the angle $\theta$ in Figure 1d). We calculate $\mathbf{d_{actual}}$ by blending

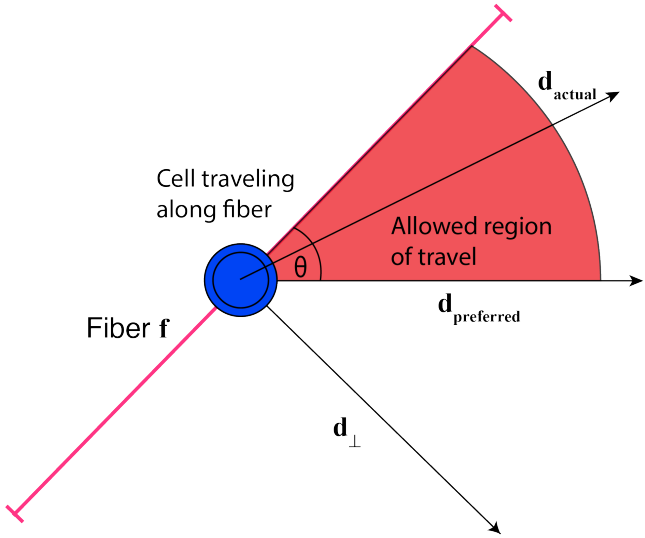


Supplementary Figure 1: Schematic for mathematical model of cell motility and ECM orientation interactions. Cell shown in blue. See 8, 10, and 12 for variable explanations.

the basis vectors using the cell's ECM sensitivity parameter $s$ and local ECM element's anisotropy $a$ as follows:

$$\mathbf{d_{actual}} = (1-\gamma)C_1\mathbf{d}_\perp + C_2\mathbf{f}, \tag{8}$$

where $\gamma$ is the effective ECM influence parameter. This captures both cell sensitivity and magnitude of ECM fiber alignment (signal strength):

$$\gamma = a(\mathbf{x_i}) \cdot s_i. \tag{9}$$

$s_i$ and $a(\mathbf{x_i})$ are a parameter of cell $i$ and anisotropy at that location respectively. The other terms in Equation 8, the coefficients $C_1$ and $C_2$ and basis vector $\mathbf{d}_\perp$, are calculated by decomposing $\mathbf{d_{preferred}}$ and basic trigonometry. For brevity, we will drop location and indexing of cells unless needed for clarity.

We find $\mathbf{d}_\perp$, using the trigonometric relationship $\mathbf{A} \cdot \mathbf{B} = ||\mathbf{A}||||\mathbf{B}||\cos\,\theta$. Letting $\mathbf{f}$ and $\mathbf{d_{preferred}}$ be unit vectors and $\theta$ being the angle between them, the relationship simplifies to:

$$\mathbf{d_{preferred}} \cdot \mathbf{f} = \cos\,\theta. \tag{10}$$

Scaling $\mathbf{f}$ by that dot product, we get the component of $\mathbf{d_{motility}}$ that points along $\mathbf{f}$. Subtracting that result from $\mathbf{d_{motility}}$, we obtain a vector perpendicular to $\mathbf{f}$ as follows:

$$\mathbf{d}_\perp^{'} = \mathbf{d_{preferred}} - (\mathbf{d_{preferred}} \cdot \mathbf{f})\mathbf{f} \tag{11}$$

with normalization producing the unit vector $\mathbf{d}_\perp$ seen in Equation 8 and Figure 1d.

Note also that $\mathbf{d_{preferred}}$ can be decomposed as follows:

$$\mathbf{d_{preferred}} = C_1\mathbf{d}_\perp + C_2\mathbf{f} \tag{12}$$

with $C_1$ and $C_2$ the same as in Equation 8. They are determined via dot product and again, we take advantage of the terms being unit vectors:

$$\begin{aligned}\mathbf{d_{preferred}} \cdot \mathbf{d}_\perp &= (C_1\mathbf{d}_\perp + C_2\mathbf{f}) \cdot \mathbf{d}_\perp \\ &= C_1\mathbf{d}_\perp \cdot \mathbf{d}_\perp + C_2\mathbf{f} \cdot \mathbf{d}_\perp \\ &= C_1. \end{aligned} \tag{13}$$

Likewise, by dotting both sides of Equation 12 by $\mathbf{f}$, we obtain $C_2$ as follows:

$$\begin{aligned}\mathbf{d_{preferred}} \cdot \mathbf{f} &= (C_1\mathbf{d}_\perp + C_2\mathbf{f}) \cdot \mathbf{f} \\ &= C_1\mathbf{d}_\perp \cdot \mathbf{f} + C_2\mathbf{f} \cdot \mathbf{f} \\ &= C_2. \end{aligned} \tag{14}$$

With that, all required parts of Equation 8 are determined, letting $\mathbf{d_{preferred}}$ be calculated. Note that if the effective influence parameter $\gamma$ is zero, Equation 8 becomes Equation 12. Likewise, when $\gamma$ is one, its maximum value, $\mathbf{d_{preferred}}$ equals $\mathbf{f}$.

In the case that $\mathbf{d_{preferred}}$ is parallel to $\mathbf{f}$, $\mathbf{d}_\perp^{'}$ from Equation 11 is the zero vector. We assume the norm of the zero vector to be zero. With that set, the calculations will proceed as normal.

Note that there are two possibilities on how to interpret $\mathbf{d_{actual}}$:

**A:** The cell senses its environment, determines direction of travel along the fibers, and all cell effort goes into that motion.

**B:** The cell attempts to move both along the fibers and along its preferred direction, wasting effort in the process.

These two interpretations lead to either normalizing $\mathbf{d_{actual}}$ (Option **A**) or letting the cell direction vector lose magnitude by not normalizing $\mathbf{d_{actual}}$ (Option **B**). For the purposes of this work, we choose Option **B** and do not normalize $\mathbf{d_{actual}}$.

### Constitutive relations to determine $\mathbf{d_{preferred}}$

To determine $\mathbf{d_{preferred}}$ in Equation 8, we extend the motility model of [24]'s motility model.

#### *Model I: Chemotaxis based motility*

To determine $\mathbf{d_{preferred}}$ for chemotactically motivated cells, we use the following equation from [24]:

$$\mathbf{d_{preferred}} = (1 - b) \cdot \mathbf{d_{random}} + b \cdot \mathbf{d_{chemotaxis}} \tag{15}$$

where $\mathbf{d_{random}}$ is a randomly generated unit vector, $\mathbf{d_{chemotaxis}}$ is a unit length microenvironment-derived direction, such as the gradient of a cell-required substrate, and the scalar $b$, running from 0 - 1, is the directional bias parameter that sets the balance between random, 0, and completely

biased cell motility, 1. $\mathbf{d_{preferred}}$ is the cell selected motility direction and may be combined with local fiber orientation to produce the final cell motility direction.

### *Model II: ECM and chemotaxis based motility*

To produce behaviors of both gradient and ECM following, we reformulated Equation 15 and replace the chemotactic bias with the local ECM anisotropy:

$$\mathbf{d_{motility}} = (1-a)\cdot\mathbf{d_{random}} + a\cdot\mathbf{d_{chemotaxis}} \tag{16}$$

Here, $a$ replaces the bias parameter in setting the random versus chemotactic behavior. When combined with the cell-ECM interactions, this model effectively enables a cell to only be chemotactic when in remodeled ECM.

### *Model III: History based motility*

To generate a memory or hysteresis based motility, we alter the model in Equation 15 to include the anisotropy from the location of the most recent motility update, $a(\mathbf{x}_{\text{previous}})$, and a different bias parameter, $b_{\text{memory}}$, as follows:

$$\delta = a(\mathbf{x}_{\text{previous}})\cdot b_{\text{memory}} \tag{17}$$

$$\mathbf{d_{preferred}} = (1-\delta)\cdot\mathbf{d_{random}} + \delta\cdot\mathbf{d_{previous\ preferred}}. \tag{18}$$

$\delta$ incorporates both how sensitive the updated cell motility is to its most recent direction, $\mathbf{d_{previous\ preferred}}$ as well as how much fiber orientation there was to "remember" from the position of the most recent motility update. This model is included for the sake of completeness but not is not explored in this study.

### *ECM density*

We use the following relationship to incorporate the influence of ECM density $\rho$ on cell speed:

$$s_{\text{cell}} = \begin{cases} 0 & \text{if } \rho \le \rho_l \\ S_{max}\frac{\rho-\rho_l}{\rho_{ideal}-\rho_l} & \text{if } \rho_l < \rho \le \rho_{ideal} \\ S_{max}\frac{\rho-\rho_h}{\rho_{ideal}-\rho_h} & \text{if } \rho_{ideal} < \rho < \rho_h \\ 0 & \text{if } \rho \ge \rho_h \end{cases} \tag{19}$$

where $\rho$ is the local ECM density, $S_{max}$ is the maximum cell migration speed, $\rho_l$ is the ECM threshold density above which cells have non-zero speed, $\rho_h$ is the ECM threshold density above which cells cannot move, and $\rho_{ideal}$ is the ECM density of maximum speed.

This form simulates that in an actual fibrous environment a cell cannot move either when density is too low, due to a lack of fibers to grab onto for propulsion, or when density is too high, meaning the ECM is too dense for the cell to pass through. Other polynomials or curves derived from fitting to data could be used in place of this form. We choose it to be a minimum example of a tunable, potentially asymmetric curve with a local maximum.

## 7.3 Detailed parameter values

See Tables 2 to 5 for cell invasion parameters. Unless indicated otherwise, parameters are at default values for Physicell 1.4.1.

| Parameter | Value | Range |
|---|---|---|
| Adhesion strength | varies | 2.5, 5.0, 10 $\mu$m/min |
| Repulsion strength | 25.0 $\mu$m/min | - |
| Base cell speed | varies | 0.25, 0.5, 1.0 $\mu$m/min |
| Oxygen uptake | 10 mmHg | - |
| Rate of proliferation | 0 min$^{-1}$ | - |
| Rate of death | 0 min$^{-1}$ | - |
| Chemotactic bias | Leaders - 0.95, followers - dynamic | - |
| Persistence time | 10 min | - |

**Table 2**: Cell-level parameters specific to the cell invasion model. Unless otherwise stated, parameters are at default values. Note - In the supplementary, some followers have a chemotactic bias of 0.05.

| Parameter | Value |
|---|---|
| Oxygen diffusivity | 100,000 $\mu$m$^2$/min |
| Oxygen decay constant | 0.1 mmHg oxygen/min |
| Boundary condition type | Dirichlet |
| Boundary condition value | 38 mmHg oxygen |
| Computational mesh element size | 20 by 20 by 20 $\mu$m$^3$ |

**Table 3**: Biotransport and chemical microenvironment parameters for cell invasion model.

| Parameter | Value |
|---|---|
| Initial anisotropy | 0 |
| Initial density | 0.5 |
| Initial orientation | random |
| Fiber realignment rate (rate of change in anisotropy) | 0.001 min$^{-1}$/0.004 min$^{-1}$ |
| Fiber reorientation rate | 1 min$^{-1}$/4 min$^{-1}$ |
| ECM element size | varies |

**Table 4**: ECM initial conditions and remodeling parameters for all simulations, with the exception of the changes to ECM element size. Simulations in main body of text were produced with cubic elements with side length of 20 $\mu$m. Supplemental materials included results with rectangular elements of dimensions 40 $\mu$m by 40 $\mu$m by 20 $\mu$m and 80 $\mu$m by 80 $\mu$m by 20 $\mu$m respectively as well as cubic elements with side length of 20 $\mu$m. Element sizes are uniform and constant throughout any given simulation.

| Parameter | Value |
|---|---|
| Initial organoid radius | 175 $\mu$m |
| Computational domain size | 1600 $\mu$m by 1600 $\mu$m |
| Pre-mechanics microenvironment conditioning duration | 10 min |
| Cell fraction of leaders | 0.05 (main results), 0.10 (supplemental material) |

**Table 5**: Tissue level parameters for cell invasion model.

## 7.4 Links to supplemental videos

### 7.4.1 Figure 2: Highlights of individual aspects of the cell-ECM interactions

Figure 2a - Cell March

Figure 2b - Circular ECM with no gradient

Figure 2c - Circular ECM with chemical gradient.

### 7.4.2 Figure 3: Communication of cell path through environmental modification produces invasive, stigmergic cell behavior

Figure 3a - Writing only

Figure 3b - Reading only

Figure 3c - Writing and reading

### 7.4.3 Figure 4: Multiple behaviors are produced with cell-ECM model

Figure 4a - Speed = 1.0 $micron/\text{min}$

Figure 4b - Speed = 0.5 $micron/\text{min}$

Figure 4c - Speed = 0.25 $micron/\text{min}$

### 7.4.4 Figure 5: Collective migration is retained in the context of noisy communication videos

Figure 5a - Instant signal writing (same data as Figure 4b)

Figure 5b - Non-instant signal writing

### 7.4.5 SM Figure 2: Highlights of individual aspects of the cell-ECM interactions

SM Figure 2 - Split ECM with chemotaxis

### 7.4.6 SM Figure 3: Collective migration requires sufficiently fast remodeling

SM Figure 3a - Instant signal writing (same data as Figure 4b and 5a

SM Figure 3b - Loss of collective migration due to decreased remodeling rates

## 7.5 Supplemental Figures

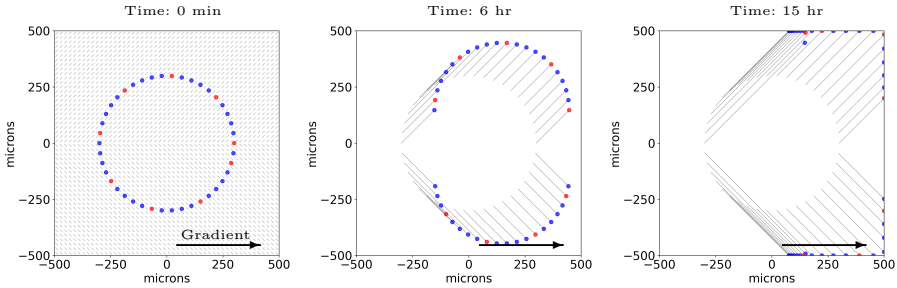


Supplementary Figure 2: **Highlight of individual aspects of the ECM-cell interactions: ECM orientation and cell chemotaxis** A combination of cues directing cell motility: ECM orientation (45° in the top of the domain and -45° in the bottom) and chemical gradient (to the right). The small black arrows trailing the cells show the positional history of each cell. The cell position is marked every 6 simulated minutes. Red and blue cells are identical; the coloring was added only for visual contrast. See link to video in Section 7.4.5.

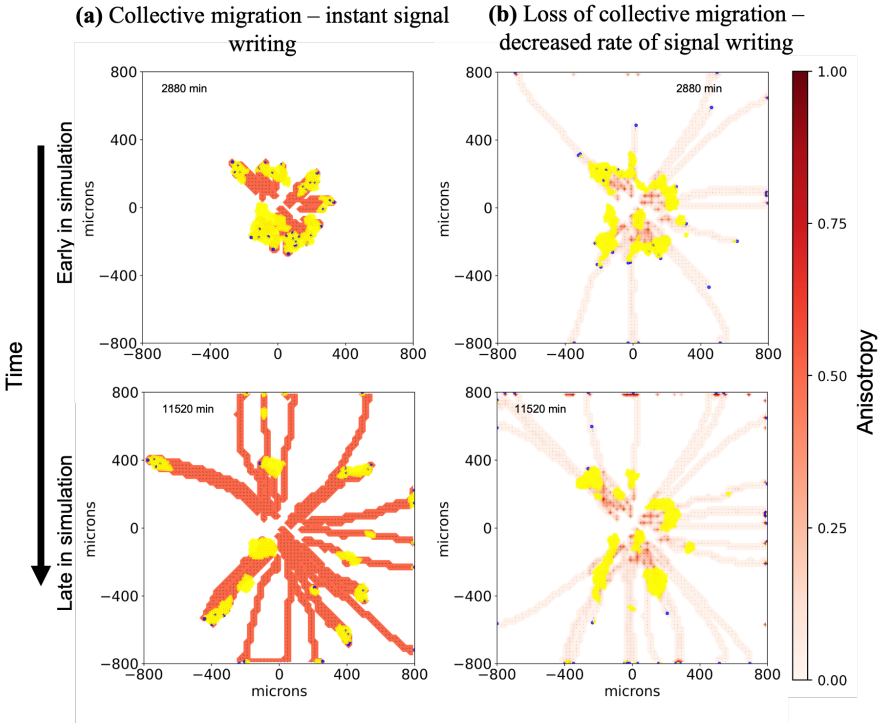


Supplementary Figure 3: **Collective migration requires sufficiently fast remodeling parameters** Figure 5a with instantaneous ECM remodeling contrasts with with **5**b which has relaxed the instantaneous signal writing and has remodeling rates slower than that in Figure 5b. Fiber realignment rate: 0.001 $\text{min}^{-1}$, fiber reorientation rate: 1 $\text{min}^{-1}$. See link to video in Section 7.4.6.